Nanochem Res 8(1): 1-22, Winter 2023

RESEARCH PAPER

Dye removal from aqueous solution by magnetic nanocomposites of metal-organic framework with $NiFe_2O_4$@SiO_2

Mehrnaz Gharagozlou*, Mehdi Ghahari, Maryam Heydari

Department of Nanomaterials and Nanocoatings, Institute for Color Science and Technology, Tehran, Iran.

ARTICLE INFO

Article History:
Received 20 Jul 2022
Accepted 23 Jan 2023
Published 17 Jan 2023

Keywords:
Metal-organic framework
Methylene blue
Dye removal
Wastewater
Magnetic nanocomposites

ABSTRACT

Magnetic nanocomposites of nickel ferrite nanoparticles, uniformly dispersed in the silica matrix, were synthesized successfully by a sol-gel process using tetraethyl orthosilicate (TEOS) and metallic nitrates as precursors. $NiFe_2O_4$@SiO_2@HKUST-1 magnetic nanocomposites were synthesized and characterized by transmission electron microscopy (TEM), scanning electron microscopy (SEM), X-ray diffraction (XRD), Fourier transform infrared spectrometry (FTIR), vibrating sample magnetometry (VSM), nitrogen adsorption porosimetry, Thermal Analysis (TGA), photoluminescence analysis, and UV-visible. The more acidic pHs and lower concentrations of the dye solution, the less the dye molecules are present in the solution; therefore, the pore volumes and surface areas will be filled slowly and with higher removal efficiency. Magnetic nanocomposite of metal-organic, ferrite-nickel, and silica framework have high efficiency and absorbability for cationic dyes such as methylene blue. Within 60 minutes, approximately 98% of the dye molecules were removed using the magnetic metal-organic framework nanocomposite 30% $NiFe_2O_4$@SiO_2@HKUST-1 under optimum condition. Adsorption isotherms, kinetics, and adsorption studies have shown that R^2 is the most frequent Freundlich isotherm, which means that the adsorption process was mainly multilayered on heterogeneous surfaces of the metal-organic framework nanocomposites.

How to cite this article
Gharagozlou M., Ghahari M., Heydari M. Dye removal from aqueous solution by magnetic nanocomposites of metal-organic framework with $NiFe_2O_4$@SiO_2. . Nanochem Res, 2023; 8(1): 1-22 DOI: 10.22036/ncr.2023.01.001

INTRODUCTION

Today, the spread of chemistry-related inventions and discoveries have had a significant impact on human civilization. Chemical processes pose a serious threat to both human health and environment because of how crucial chemistry is to modern society and numerous businesses. Today, a variety of methods are used to synthesize materials that must be compatible with the human body. However, such methods cause environmental problems [1, 2].

One of the most important methods of material synthesis is the green synthesis method. Green chemistry is the design of chemical products and processes which reduces or eliminates the use and production of harmful substances to human health and the environment. It is one of the most significant methods of synthesis because the main goal of green chemistry is to reduce the pollution caused by the synthesis as well as the use of biocompatible materials and renewables [3]. Other goals of green chemistry include using healthier chemical processes rather than current trends, conducting chemical reactions in safer conditions, producing healthier products, and increasing energy and reaction efficiencies. Today, it also designs processes that require less auxiliary materials, especially

* Corresponding Author Email: *gharagozlou@icrc.ac.ir*

chemical solvents [4]. Sometimes chemical and biochemical reactions are carried out together to make the final process healthier and to reduce their side effects as much as possible [5-7]. Therefore, in this paper, in addition to using biocompatible and renewable materials, the synthesis method was designed and selected in such a way that it has biological processes and minimal biological side effects. As well as nanocomposites synthesized in this way, it can separate environmental pollutants. For thousands of years, dyeing materials have been widely used in industries such as textiles, dyeing, pigments and many others [8].

As a result, dyes are one of the main sources of environmental contamination that can lead to skin diseases, respiratory problems, and the risk of cancer [9,10]. For this reason, it is paramount to effectively remove the dyes from the sewage and to ensure that the water is treated well and discharged to the current waterbed. Various methods have been utilized so far to effectively remove hazardous substances from aqueous solutions; such methods include biological, physical, oxidation, electrical coagulation, photocatalytic, and chemical degradation [11-14]. Particularly important are ternary magnetic nanocomposites, containing metal-organic frameworks, magnetic ferrite nickel, and silica nanoparticles.

In recent years, the use of metal-organic frameworks (MOFs) and magnetic nanocomposites have become significantly important due to their application in various fields such as sorbents [15], biomedicine [16], magnetic fluids [17], catalysts [18], biotechnology [19], information storage and environmental correction [20,21]. Metal-organic frameworks are a group of porous cordial polymers which have various metal centers and bridges leading to the formation of various structures [22-25]. Among magnetic nanoparticles, ferrite nanoparticles can be used in the separation and extraction of various organic and inorganic species, especially environmental pollutants; this is due to their special properties such as ease of synthesis, high volume surface area, magnetic properties, the ability to easily and quickly extract different species just by applying an external magnetic field [26-30].

By reducing the size of magnetic nanoparticles, the surface-to-volume ratio increases; as a result, their reactivity increases and their magnetic properties are more affected by the surface. Therefore, magnetic nanoparticles are more reactive than mass magnetic particles. Thus, in various applications, they must be protected against corrosion and other reactions [31]. The presence of a protective layer as a shell on a nanoparticle, in addition to protecting the nanoparticles from reactions, prevents them from sticking together and clumping [32]. In this research, silicon (SiO_2) was used as a coating which not only stabilizes nickel ferrite nanoparticles in solutions, but also allows the formation of bonds on the surface of nickel ferrite nanoparticles by creating different ligands [33].

For this reason, magnetic nanoparticles were employed to synthesize nanocomposite acting smart and to be controlled by an external magnetic field. Because the magnetic nanoparticles have a low surface area, they absorb a small amount of environmental pollutants; therefore, metal-organic frameworks were placed on them to increase the surface area and maximize the adsorption capacity of these particles [34-36]. One of the applications of metal-organic frameworks is their use in the absorption and separation of gases and liquids [37,38].

Abdi et al. synthesized magnetic metal-organic framework nanocomposite (ZIF-8@SiO_2@$MnFe_2O_4$) by co-synthesis, and after characterization the cationic dye malachite green and the anionic dye methyl orange were removed. They found that the synthesized nano-composite magnetic metal-organic framework can remove and absorb 92.5% of malachite green, cation dye and 5.9% of methyl orange dye from dye solutions [39]. Thi Minh et al. synthesized the magnetic metal-organic framework (Fe_3O_4@MIL-101) and then proceeded to photo-catalytically degrade the methylene blue dye [40]. Tingting et al. were able to remove rhodamine B6 dyes from the dyeing wastewater by synthesizing single-phase porous magnetic composite Ni@MOF-74(Ni) [41].

Hosseinzadeh et al. removed the methylene blue dye by synthesizing a metal-organic framework (Fe-BTC). The metal-organic framework synthesized in the presence of hydrogen peroxide, UV light and ultrasonic device showed high photocatalytic properties and that the dye removal mechanism follows Fenton's method [42]. When ferrite magnetic nanoparticles are introduced into the substrate of metal-organic frameworks, they induce the magnetic properties of the resulting nanocomposite. Consequently, the synthesized magnetic nanocomposite functions as a stronger inhomogeneous adsorbent and is easily used for the removal of toxic dyes and pollutants; ultimately, it can be easily separated with an external magnet,

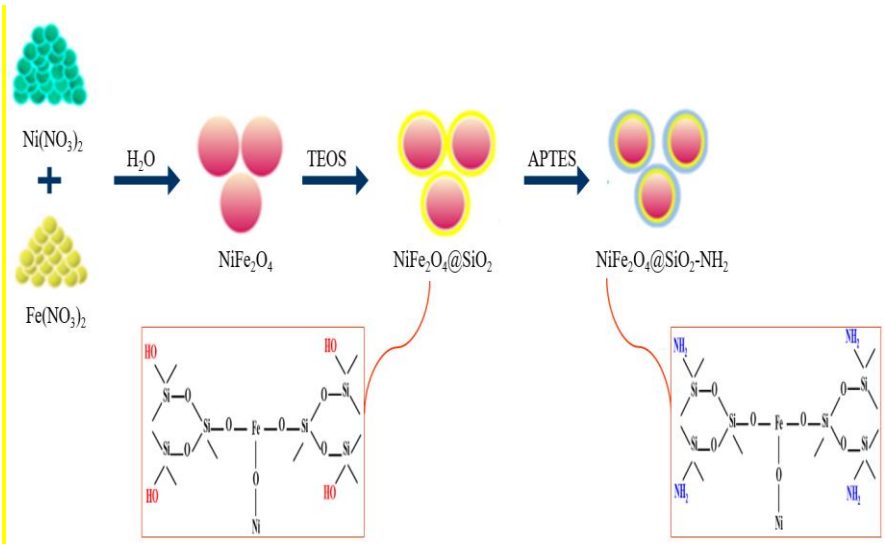

Fig. 1. Schematic of synthesis of nickel ferrite on silica substrate $NiFe_2O_4@SiO_2$

which saves time, energy and costs.

In this paper, $NiFe_2O_4@SiO_2$@HKUST-1 adsorbent was prepared by an in-situ self-assembly method, which is one of the green synthesis methods, and identified by elemental analysis. The application of synthesized samples in methylene blue pollutant adsorption and the influence of time and pH factors were investigated. Adsorption isotherms, kinetics and adsorption mechanisms and other mentioned thermodynamic parameters on magnetic nanocomposites were thoroughly investigated and analyzed.

EXPERIMENTAL METHOD

Chemicals and methods

All chemicals used in this article are Merck Brand including methylene blue, MB, as a dyeing agent prepared from Ciba company. 3-Aminopropyl triethoxy silane, APTES, with the purity percentage of 98% were purchased from Merck Germany. Iron (III) nitrate, nickel (II) nitrate, copper (II) nitrate with the purity percentage of 99% were purchased from (Temad company, Iran). Ethanol solvent 99.8% and tetraethyl orthosilane and benzene1,3,5-tricarboxylic acid were purchased from Merck Germany. Glutaric anhydride, GA, with the purity percentage of 99% and deionized water were purchased from Arya Chemists company.

After the synthesis, the magnetic metal-organic framework nanocomposite (NiFe2O4@SiO2@HKUST-1) was evaluated. The synthesized samples were evaluated by using X-ray diffraction pattern for structural analysis and phase-type determination (Philips PNA analytical device, XRD), Fourier transform infrared spectroscopy for molecular structure and energy determination of chemical bonds (PerkinElmer), scanning electron microscopy (LEO 1455VP SEM) for fine analysis structural, transmission electron microscopy (TEM) to determine microstructures and orientation of crystals, vibrating sample magnetometer to measure the magnetic properties of compounds, using thermal analysis (TGA) to analyze the physical properties of materials under higher temperature and UV-Vis spectrophotometer.

Synthesis of nickel ferrite on silica substrate $NiFe_2O_4@SiO_2$

This step was in accordance with the synthesis method for nickel ferrite nanocomposites in silica media reported in other articles [18]. First 6.2 gr of nickel nitrate and 17 gr of iron nitrate were dissolved each in 10 ml of deionized water and were refluxed and stirred well with a magnetic stirrer for 30 minutes until complete mixing. Next, 60 ml of tetraethyl orthosilicate (TEOS) was poured into 50 ml of ethanol and 10 ml of water while the pH was decreased using acidic hydrochloric acid. Then, the solution was poured dropwise into a decanter. The solution was allowed to be stirred for 2 hours until it was fully mixed. In the third step, the contents of the balloon were poured into the crystallizer and placed partially in the exposure of the air for 7 days and alcogel was synthesized. After 7 days, the synthesized alcogel was incubated in the oven at 110 °C for 24 hours until dried and zerogel was

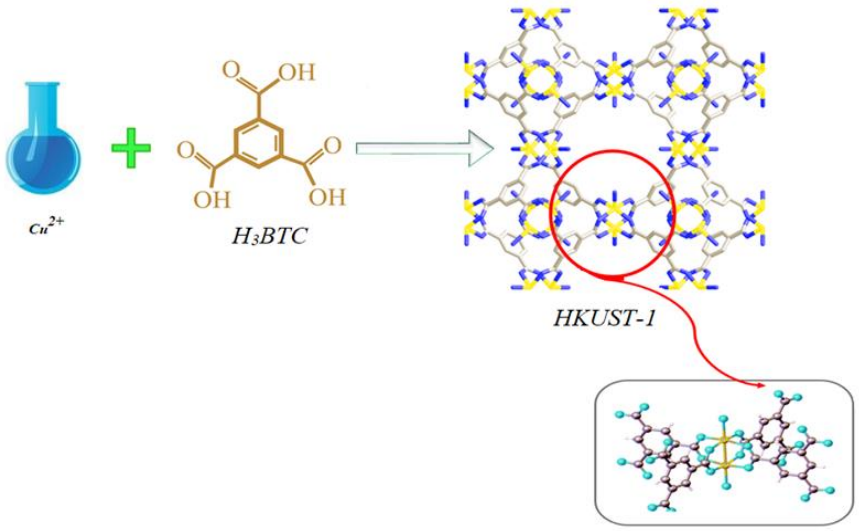

Fig. 2. Schematic of synthesis of the metal-organic framework HKUST-1

synthesized. Zerogel was then calcined for 2 hours in an 800 °C oven at a ramping rate of 10 °C /min in ambient atmosphere medium. Finally, the product was milled by a satellite mill and was named Powder (F-S) (Fig 1).

Synthesis of the metal-organic framework HKUST-1

0.84 gr of BTC ligand and 1.75 gr of copper (II) nitrate in 50 ml of ethanol was under agitated reflux conditions for 3 h, which formed a blue solid precipitate. Then the resulting solid precipitate was exposed to ambient temperature for 48 h. It was then separated by centrifugation and washed with water and ethanol and the precipitate was dried using the oven at 100 °C for 12 h (Fig 2) [20].

Synthesis of magnetic metal-organic framework nanocomposites $NiFe_2O_4$@SiO_2@HKUST-1

The first step was dispersing 1 gr of nickel ferrite prepared in the previous step with 50 ml ethanol and then adding 2 ml of APTES, and allowing it to reflow for 6 hours under reflux conditions at 80 °C for 6 h. The resulting sediment was separated using a magnet. The second step was re-dispersing the isolated nanoparticles with 30 ml of ethanol and then adding 3 gr (GA) and re-mixing under reflux for 3 h at 40 °C. After the required time, the nanoparticles were collected and washed with distilled water. The third stage was pouring 1 gr of the resulting powder from the second stage with 6.04 gr of copper nitrate and 4.72 gr of H_3BTC ligand and 60 ml of distilled water in the balloon and again under reflux conditions at 100 °C for 8 hours and followed by stirring vigorously. The precipitate from the wash was placed in a vacuum oven at 150 °C for 10 hours to dry the precipitate (Fig 3).

All synthesized magnetic metal-organic frameworks nanocomposites are presented in Table 1. Nickel ferrite nanocomposites embedded in silica substrate with the weight ratios of x ($NiFe_2O_4$)/ (100-x) SiO_2 which (x = 10, 30 and 50 wt.%) was synthesized according to the synthesis method mentioned in Section 2-2. Then their magnetic metal-organic frameworks were synthesized and identified by the synthesis method mentioned in section 2-4.

Dye decolorization

To investigate the bleaching process of methylene blue cationic dye, a solution of methylene blue dye (10 mg / L) was prepared. 100 ml of it was collected as a sample and 0.1 gr of synthesized nanocomposite in the presence of hydrogen peroxide was added and the entire solution was subjected to ultrasonication at room temperature for a certain period of time. Methylene blue concentration was measured at different times using a UV-vis light spectrometer. Finally, by using equations (1) and (2) the removal percentage of methylene blue dye and the adsorption capacity of the magnetic organic-metallic framework composite were calculated and determined, respectively.

$$\%R = (C0 - Ct / C0) \times 100 \quad (1)$$

$$qt = (C0 - Ct)\, V/m \quad (2)$$

Table 1: Introducing sample names.

Formulation	Abbreviation	Identification data in synthesis file
$NiFe_2O_4$10%@SiO_2@HKUST-1	F.S.MOF-1	
$NiFe_2O_4$30%@SiO_2@HKUST-1	F.S.MOF-2	$NiFe_2O_4$@SiO_2@HKUST-1
$NiFe_2O_4$50%@SiO_2@HKUST-1	F.S.MOF-3	
HKUST-1	MOF	MOF
$NiFe_2O_4$ 10%@SiO_2 800	BE	
$NiFe_2O_4$ 30%@SiO_2 800	BD800	$NiFe_2O_4$@SiO_2
$NiFe_2O_4$ 50%@SiO_2 800	BH	

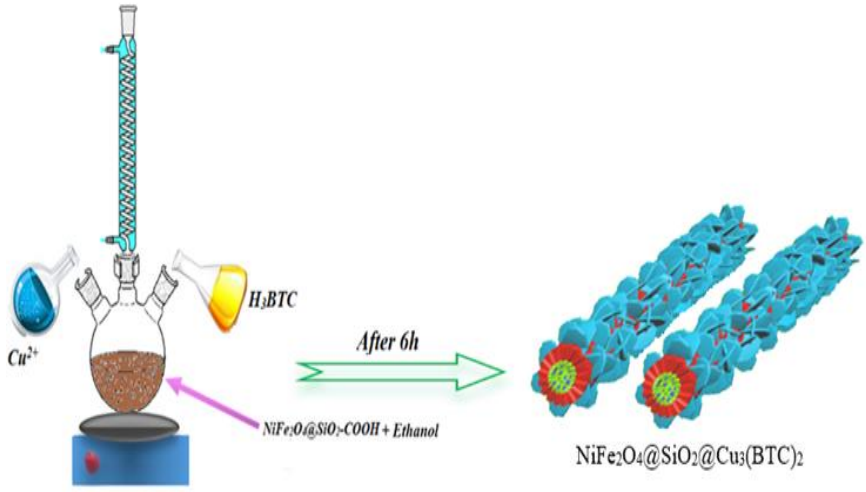

Fig. 3. Schematic of synthesis of magnetic metal-organic framework nanocomposites

Where C_0 and C_t are the initial concentration of dye solution and concentration of dye solution at time t; V is the volume of solution in liters; m denotes the amount of nano composite (gr), and q_t is the adsorption capacity of nanocomposite magnetic metal-organic framework in terms of mg. g^{-1}. Finally, the effect of different parameters on the removal of methylene blue dye was studied.

RESULTS AND DISCUSSIONS

XRD Analysis

Ternary metal-organic nanocomposites and ferrite nickel were synthesized on silica substrate ($NiFe_2O_4$@SiO_2@HKUST-1) by the in-situ self-assembly method. This method means that the components of the system are arranged to form a larger unit, which can occur spontaneously either directly or indirectly through the environment due to specific reactions. Fig. (4-a) shows the diffraction pattern of the synthesized samples which contains nanoparticles ($NiFe_2O_4$), amorphous SiO_2 particles, and a metal-organic framework containing copper (HKUST-1). These diffraction patterns are consistent with other reports [43-45]. An increase in concentration ($NiFe_2O_4$) and a decrease in silica substrate concentration are clearly visible at peak 24 ° and sharpening of peaks ($NiFe_2O_4$). According to reports, the peaks observed in the range of 15-20 are related to the presence of a metal-organic framework containing copper. Peaks in the range of 30-40 are attributed to the presence of nickel ferrite in the silica bed which confirms the existence of a metal-organic framework containing copper (HKUST-1) and nanocomposites ($NiFe_2O_4$). The main peaks of the synthesized magnetic metal-organic nanocomposite frame include 16.05, 19.9, 42.24, 74.35, 28.37, 47.43, 57.53, 55.57, 72.62; peaks

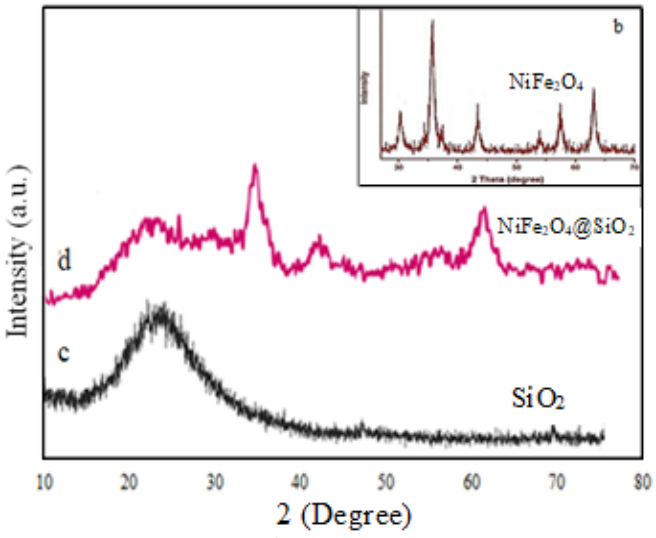

Fig. 4. a) XRD pattern of synthesized magneto-organic metal frameworks b) XRD pattern of nickel ferrite magnetic nanocomposite placed in silica substrate

related to MOF and nanoparticles ($NiFe_2O_4$) are observed in all three patterns. Fig. (4-d) illustrates the pattern of nickel ferrite nanocomposites in silica substrate compared with the reference peaks of nickel ferrite (5-b) and silica (5-c) nanoparticles [46,47]. This diffraction pattern indicates that the peaks include nickel ferrite index peaks with cubic spinel structure Fd3m which represent the plate group (2 2 7) and silica lattice index peaks which represent the plate group (2 2 0). These results indicate that the nanocomposite was synthesized correctly, and its pattern is consistent with the existing reports [46-50].

The Scherer equation (Equation 2) was used to calculate the average crystal size using the XRD model.

$$t = 0.9\lambda / \beta Cos\ \theta \qquad (2)$$

In this equation, t is the average size of crystals in nanometers; λ is the X-ray wavelength in nanometers; β is the Peak width at half the maximum height in radians, and θ is the peak location in the XRD pattern in degrees. Table 2 shows the location of the maximum peak in the XRD pattern and the average size of the crystals. In addition, the average distance between the nanocomposite crystal plates of the synthesized magnetic metal-organic frameworks is presented. After performing the calculations, it was observed that nanocomposite of magnetic metal-organic framework containing 50% ($NiFe_2O_4$ @ SiO_2 50% @ HKUST-1) has the highest crystallinity compared to 10% and 30%.

FT-IR Analysis

Fig. (5) shows the synthesized magnetic metal-organic frameworks of the FTIR spectrum. There are three spectra of magnetic metal-organic frameworks ($NiFe_2O_4$@SiO_2@ HKUST-1) containing different percentages of nickel ferrite. Many peaks observed in the spectrum of nickel ferrite magnetic nanocomposites in silica substrate ($NiFe_2O_4$@SiO_2) and the spectrum of metal-organic framework (HKUST-1) overlap and are reported [40,53]. This indicates the formation of all three magnetic metal-organic frameworks ($NiFe_2O_4$@ SiO_2@ HKUST-1) with different percentages of nickel ferrite. The presence of peaks in the area of 1580-1709 cm^{-1} is due to the presence of carboxyl (COO-) groups in the connector (BTC) and the peak in the 1163-700 cm^{-1} region corresponds to the double bond (C = C) of the aromatic group in the binder (BTC) belonging to the copper metal-organic framework (HKUST-1).

In addition, the presence of peaks in the area of 685 cm^{-1} and 744 cm^{-1} indicates silica networks and group tensile vibrations (Si-O-Si). The presence of a peak in the area of 476 cm^{-1} is related to asymmetric tensile vibrations (Cu-O) and the peak in the region of 524 cm^{-1} is attributed to tensile vibrations (Fe-O), which indicate the accuracy of the synthesis of all three compounds. It is clear that the intensity of the peaks related to the vibrations of Si-O, Cu-O, Si-O-Fe in the sample of the magnetic metal-organic frameworks containing 50 wt. %

Table 2. XRD parameters of nanocomposites

Sample	Peak position [°2θ]	Crystallite size [nm]	d-spacing [A°]
F.S.MOF-1	19.909	20.5	44.5
F.S.MOF-2	20.627	32.8	43
F.S.MOF-3	20.467	41.0	43.3

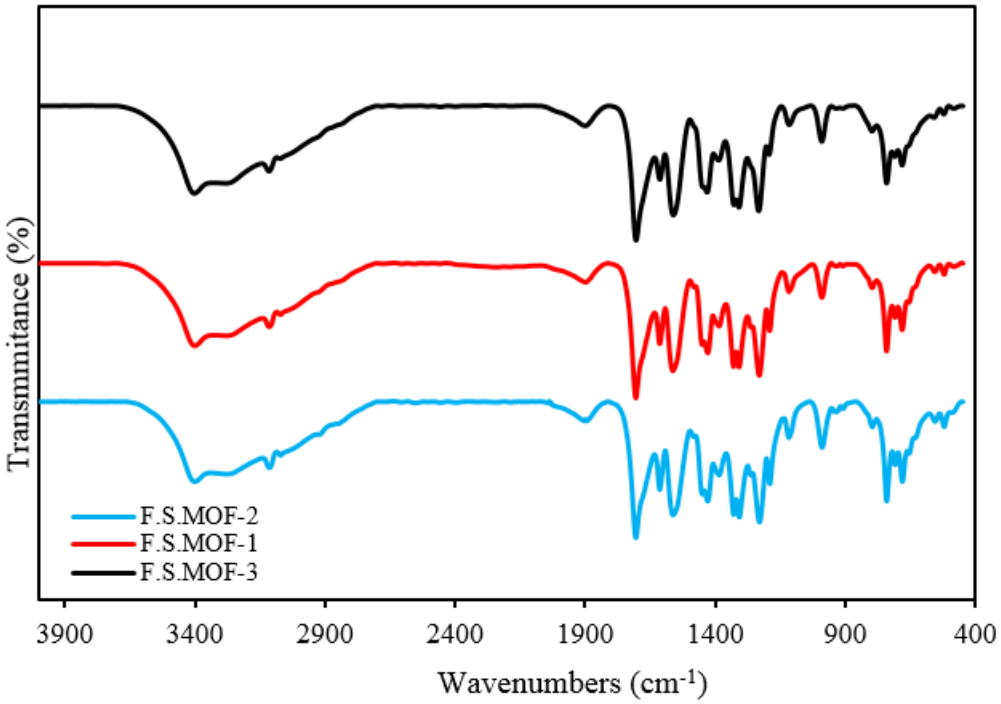

Fig. 5. FTIR analysis of magnetic metal-organic nanocomposites with different weight percentages of nickel ferrite

nickel ferrite is increased. A summary of the peaks in the infrared spectrum of the magnetic metal-organic nanocomposite framework ($NiFe_2O_4$@ SiO_2@ HKUST-1) is given in Table 3 [51-53].

Thermal Analysis (TGA)

The thermal analysis of TG, DTA, and DTG is taken from a magnetic metal-organic framework sample $NiFe_2O_4$@SiO_2@HKUST-1 with 30 wt.% and is shown in Fig (6). Thermal analyses (TG, DTA, DTG) are used to determine the thermal stability of the metal-organic framework. As can be seen, two weight reductions are observed in the thermal analysis of the graph (TG) and this is due to the synthesis process. The first weight loss reported at 150-200 °C is related to the removal of guest molecules (solvent: water and ethanol) inside the pores of the metal-organic framework and gases adsorbed on the surface are partially related to the decomposition of organic groups such as (carboxyl groups, etc.) on the surface of the magnetic nanocomposite, which is attributed to an exothermic peak in this range in the diagram (DTA) . The second weight loss in the range of 300-400 °C is usually due to the restructuring of the metal-organic framework, mostly related to the metal oxides present in the metal-organic framework. It is reported that the severe weight loss at 350 °C signifies the collapse and complete decomposition of the HKUST-1 metalorganic framework, and here the severe weight loss at 355 °C occurs when the structure of the metal-organic framework $NiFe_2O_4$@SiO_2@HKUST-1 begins to break down. It can be concluded that the metal-organic framework $NiFe_2O_4$@SiO_2@HKUST-1 has thermal stability at temperatures above about 350 °C.

Table 3: Corresponding peaks and bonds in the FTIR spectrum of a nanocomposite sample of a magnetic metal-organic framework ($NiFe_2O_4$@SiO_2@ HKUST-1)

Corresponding link	Wave number (cm^{-1})
Absorbed water or hydroxyl group	3420
Presence of organic molecules in (BTC)	1580-1709
Aromatic C = C (BTC)	1563
In-plane tensile vibrations (C-H) and flexural vibrations (O-H)	1436 and 744
Asymmetric tensile vibrations (Cu-O)	476
Octagonal and quadrilateral spinel (Ni^{2+}, Fe^{3+})	400-600
Asymmetric tensile vibrations (Fe-O)	526

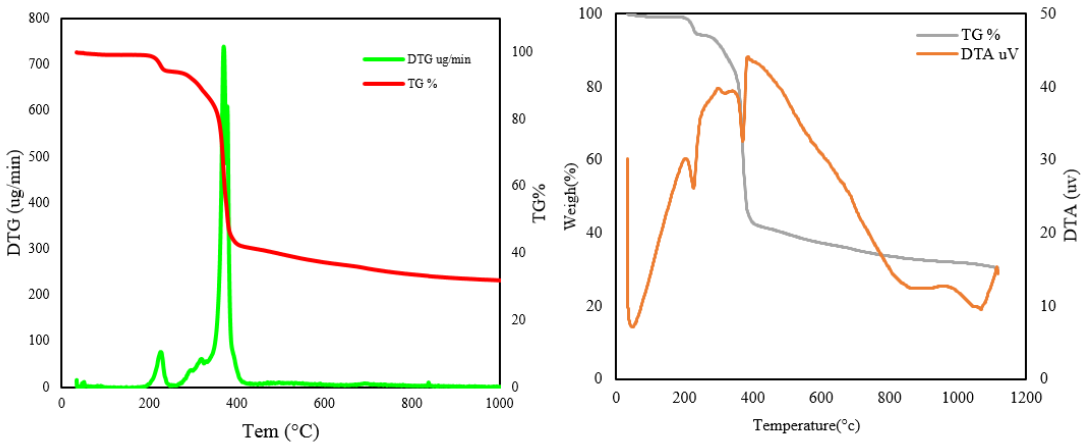

Fig. 6. thermal analysis of TG, DTA, and DTG for magnetic metal-organic framework sample $NiFe_2O_4$@SiO_2@HKUST-1 with 30 wt.% .

The peak in the DTA curve, reported in the presence of sharp peaks in region 300 and 400 °C, indicates crystal deformation and the presence of a broad peak in zone of 200-70 °C due to chemical reactions as well as the presence of a broad peak from 400 to 750 °C in thermal decomposition. The endothermic peaks can also be observed between 1100 and 750 °C due to the compacting of the metal-organic composite since mass loss occurs up to about 400 °C [54-56].

Scanning electron microscopy (SEM) analysis

Scanning electron microscopy analysis is commonly used to describe the morphology of metalorganic frameworks. These microscopic images show the outer geometry of the shape, dispersion and mixing of phases. As can be seen in Fig. (7), the synthesized $NiFe_2O_4$@SiO_2@ HKUST-1 metal-organic framework has an almost rod-like morphology such that the nickel ferrite nanoparticles in the silica substrate coalesce to form a rod-like structure.

During synthesis, the copper-containing metal-organic framework may form homogeneously around the nickel ferrite particles in the silica bed. At the highest image resolution, the presence of some pours of these metal-organic frames is visible, which is a feature of these metal-organic frameworks. These particles are similar to synthesized nanocomposites (Cu/Ni-MOF) [57-59]. Thus, the observed morphology of the synthesized metal-organic framework can confirm that the synthesized nanocomposites may have the desired properties.

Transmission electron microscopy (TEM) analysis

Fig. (8) TEM images show the synthesized magnetic metal-organic frameworks. The results of TEM analysis confirm the presence of some rod-like and hemispherical particles which are

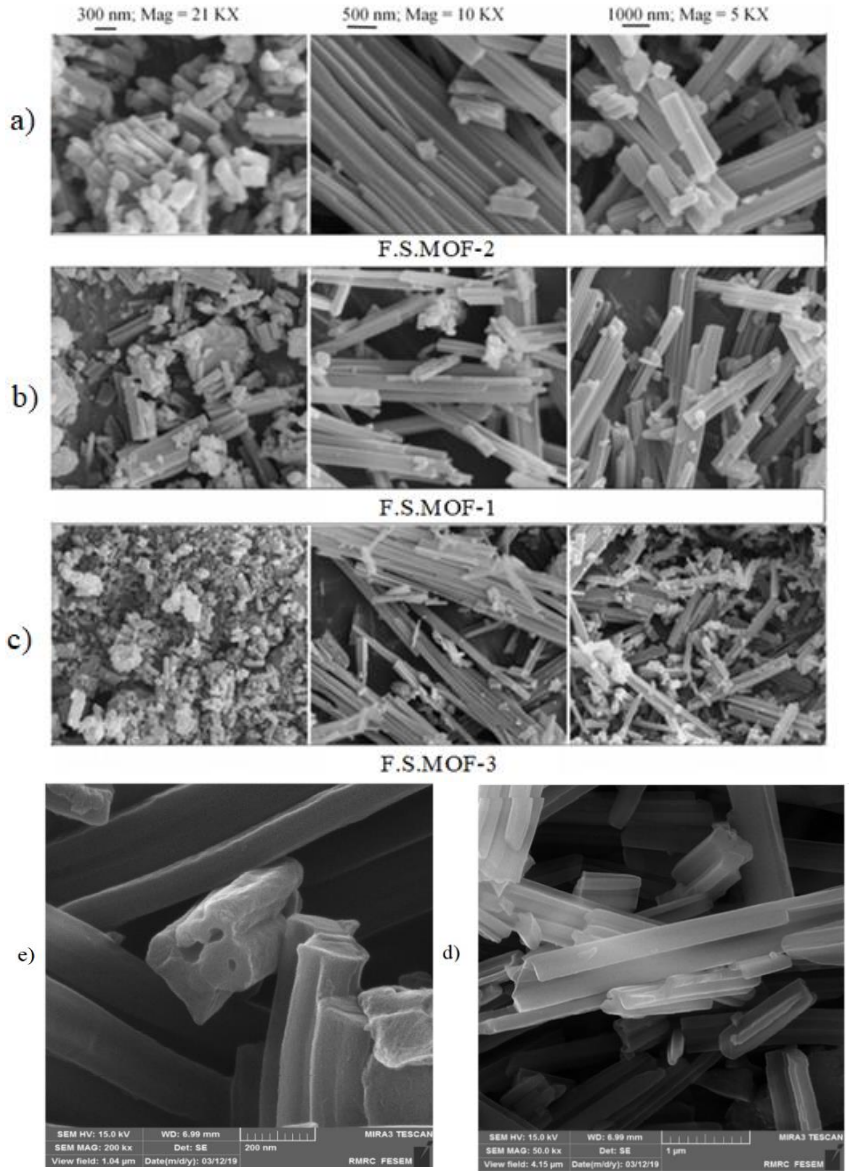

Fig. 7. SEM image of synthesized $NiFe_2O_4$@SiO_2@HKUST-1 metal-organic framework, a) 10%, b) 30% and c) 50% d) close view, e) cross section view

connected to each other. By observing the particles, it can be seen that the particles of the metal-organic framework are well crystallized and synthesized as columns (rods). These results are consistent with SEM observations. However, nickel ferrite particles located in the silica bed have a spherical morphology but their final shape changes when they are joined together by a metal-organic framework and the particles are irregularly shaped rods.

Transmission electron microscopy analysis is widely used to determine particle size, crystallographic data such as surface characteristics. This analysis is very useful and applicable for composite detection of nanoparticle-modified metalorganic frameworks because it determines nanoparticle dispersion and particle size. Fig. (8) illustrates transmission electron microscopy analysis and reveals that the metal-organic framework composite was almost rod-shaped, and nickel ferrite was deposited on the silica substrate and within the metal-organic framework network. Further, the size of these nanocomposites by weight

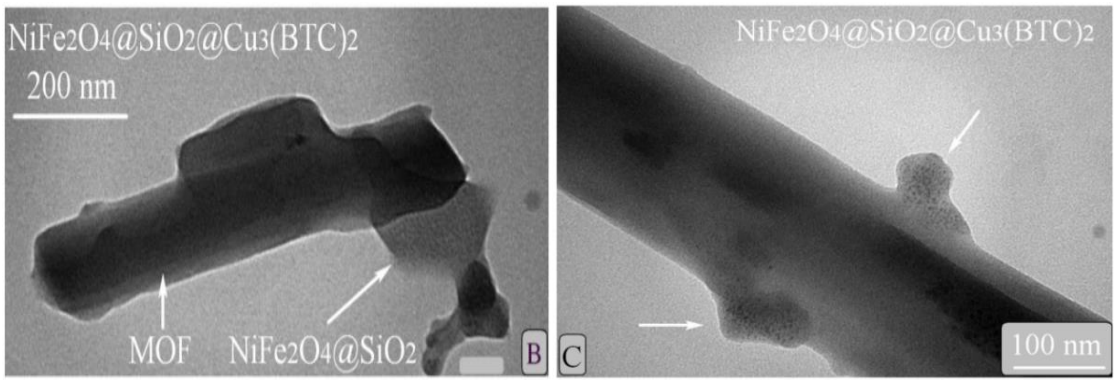

Fig. 8. TEM image of synthesized $NiFe_2O_4$@SiO_2@HKUST-1 metal-organic framework

Table 4. Nitrogen gas adsorption analysis and specific surface area

Sample	$a_{s,BET}$ (m^2/g)	d_{BET} (nm)	V_{BET} ($m^2/$)
F.S.MOF-1	38	7.3	0.0899
F.S.MOF-2	43	7	0.0757
F.S.MOF-3	90	5.1	0.1149

Table 5. Magnetic parameters of nanocomposites

Sample	M_r [emu/g]	Ms [emu/g]	Hc [O_e]
F.S.MOF-1	0.0039	0.34	0.003
F.S.MOF-2	0.016	0.87	0.04
F.S.MOF-3	0.11	2.09	0.1

percentages of 10, 30 and 50% are 20, 35 and 47 nm, respectively. The particle sizes obtained by using TEM analysis are in good agreement with the crystallite sizes of XRD results.

Nitrogen gas adsorption analysis and specific surface area

Accurate measurement of surface area and porosity of materials is important in many applications such as nanosilver, metal-organic framework, and metal nanoparticles. By knowing the average thickness of a molecule it is possible to calculate the surface occupied by the molecule and measure the amount of material absorbed and the total sample area. Fig. (9) shows the nitrogen gas adsorption analysis and specific surface area. The results regarding the nanocomposite metal-organic framework with different percentages (30, 10 and 50) of nickel ferrite, surface area, and pore volume are given in Table 4.

As shown in Table 4, by increasing the percentages of nickel ferrite from 10 to 50%, the total surface area increases, and the diameter of the pours decreases due to the presence of nickel ferrite heavy nuclei and their agglomeration [60, 61]. Fig. (10) illustrates the adsorption and desorption isotherms of nitrogen gas. As can be seen, the rates of adsorption and desorption of the samples were measured by increasing nitrogen gas at a constant temperature and by gradually decreasing it, respectively. As the vapor pressure of the material increases, the amount of material absorbed rises until a monolayer is formed on the surface. When the ratio p/p_0 is larger, it indicates that the material has very narrow pores and is well visible in the hysteresis metal-organic framework $NiFe_2O_4$@SiO_2@HKUST-1 (50%) diagram. The presence of hysteresis indicates the presence of mesoporous pores, depending on the type of hysteresis, the mesoporous form will have different shapes.

Vibrating Sample Magnetometer (VSM) Analysis

One of the most important properties of the synthesized metal-organic framework ($NiFe_2O_4$@SiO_2@HKUST-1) is its magnetic property which, having been synthesized at different weight percentages (50-30-10%) of nickel ferrite, will also have different magnetic properties which are highly dependent on the size of the nanocomposite particle. For this purpose, VSM analysis was applied to evaluate their magnetic properties, which is shown in Fig. (10) and Table 5.

Magnetic parameters including magnetic saturation, residual torque, and coercive force are listed in Table 2. The results indicate that the magnetic properties of the metal-organic

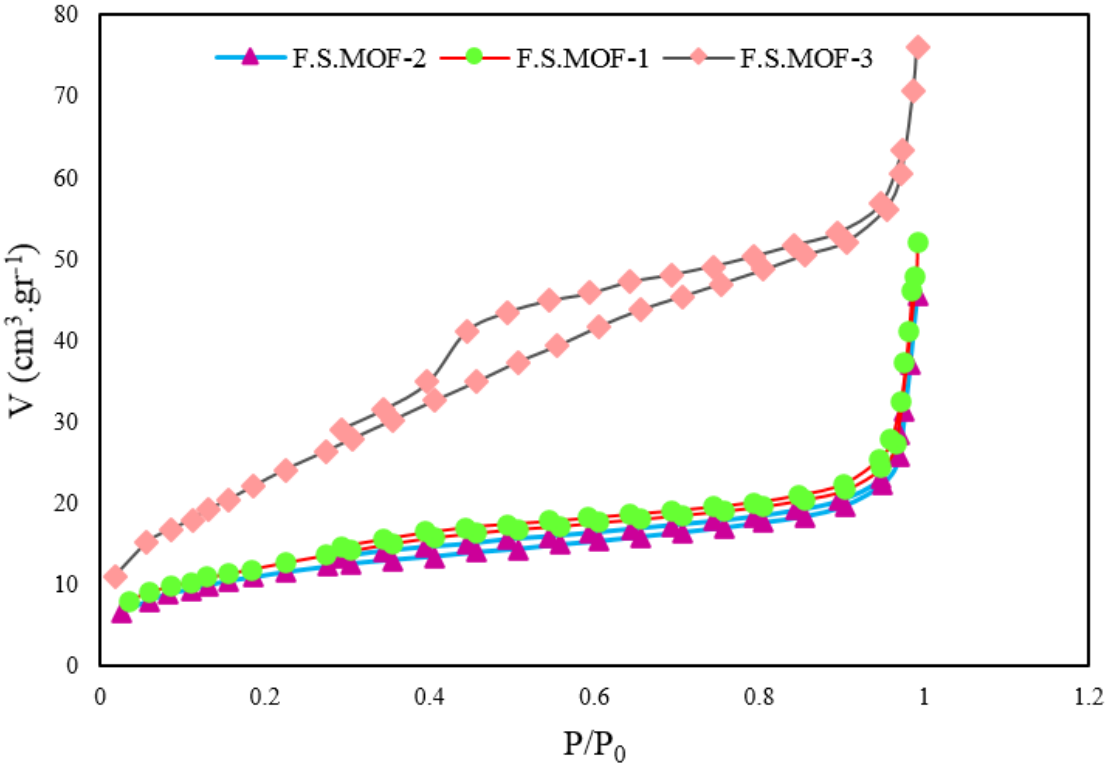

Fig. 9. Nitrogen gas adsorption analysis and specific surface area

framework rises by increasing the percentage of nickel ferrite from 10 to 50%. It can also be seen that the HKUST-1 organic metal framework alone has no magnetic properties, while by composing it with ferrite nickel, the resulting composite has a magnetic property. By not saturating the diagrams of all the samples as well as using constituents which have atoms of permanent magnetic moments such as (nickel and iron oxide), this metal-organic framework falls into the category of superparamagnetic. This is because these atoms act separately and without any interaction. As a result, they have a different and random orientation, which is influenced by an external field in an approximate direction, which is characteristic of superparamagnetic materials. These results are consistent with the previous data for nickel nanoparticles in the silica matrix and confirm the accuracy of the synthesis [62,63].

The reason for using silica in the synthesized metal-organic framework ($NiFe_2O_4$@SiO_2@HKUST-1) nanocompoite can be stated as follows: by using silica, nickel ferrite nanoparticles are dispersed uniformly in the silicon oxide matrix; this decreases the agglomeration of nanoparticles and causes their superparamagnetic properties to appear. The tendency of magnetic nanoparticles to agglomerate can be minimized by dispersing them in suitable inert matrix.

Removing dye contaminants

To investigate the application of synthesized metal-organic framework nanocomposites, its application in methylene blue pollutant adsorption was studied. Methylene blue is a cationic dye with the surface area of 1.38*0.64*0.21 nm^3 and chemical structure shown in Fig. (11) [64] Fig 12 demonstrates the decolorization of methylene blue by magnetic metal-organic framework nanocomposites.

The effect of MOF concentration on dye removal

To investigate the effect of MOF concentration on the removal of methylene blue dye, a dye solution (10 ppm) was first prepared. Then different concentrations of 30% metal-organic framework ($NiFe_2O_4$@SiO_2@HKUST-1) nanocomposite were added to the solutions and mixed with

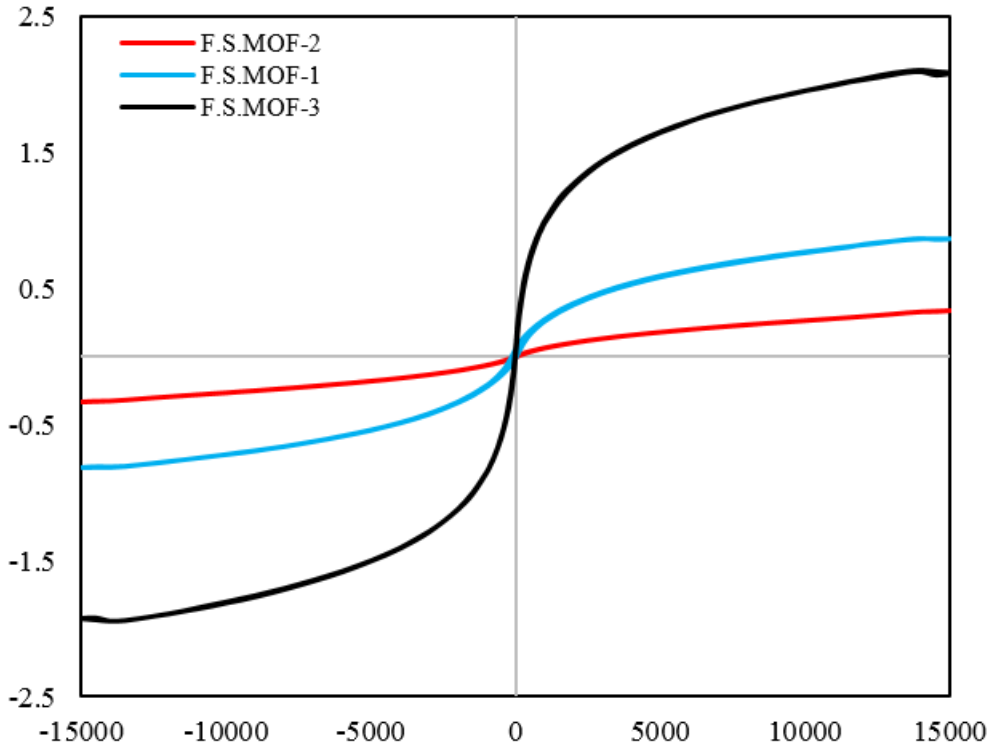

Fig. 10. Vibrating Sample Magnetometer (VSM) Analysis

ultrasonic water in the presence of oxygenated water. Then, every 10 minutes, the samples were taken, and the wavelengths were measured using spectrophotometer analysis. Fig. (13) shows the removal of methylene blue dye using various concentrations of 30% nanocomposite ($NiFe_2O_4$)@ SiO_2@HKUST-1.

As can be seen in Fig. (14), at low concentrations the removal process of dye proceeds slowly while it becomes faster with increasing nanocomposite concentration (($NiFe_2O_4$@SiO_2@ HKUST-1) 30%). For example, for 0.1 gr concentration of the nanocomposite, the dye removal was 95% after 60 min, while for 0.03 and 0.06 gr of the nanocomposite the removal was 48% and 73.5% after 70 min, respectively. According to the experimental results, the removal efficiency of the dye increased with the rise in the concentration of nanocomposites. This increase in efficiency is due to the increased concentration of the nanocomposite in the metal-organic framework of the special active surface in the solution, thus more dye molecules can be incorporated into these active sites, which improves the removal efficiency of the dye.

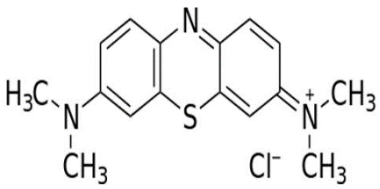

Fig. 11. Chemical structure of methylene blue dye [64].

Investigation of the effect of methylene blue dye solution concentration

First, solutions of various concentrations (10, 30, 50 ppm) were prepared in order to study the impact of methylene blue solution concentration on the removal of dye from wastewater. From each sample 100 ml sample was taken and 0.1gr of the nanocomposite ($NiFe_2O_4$@SiO_2) @ HKUST-1) (30%) was added in the presence of oxygenated water and again under ultrasonication for better mixing. After 10 minutes, the samples were collected and centrifuged, and the amount and removal efficiency were calculated using a spectrophotometer.

It can be seen in Fig. 15 that the removal efficiency in methylene blue aqueous solution

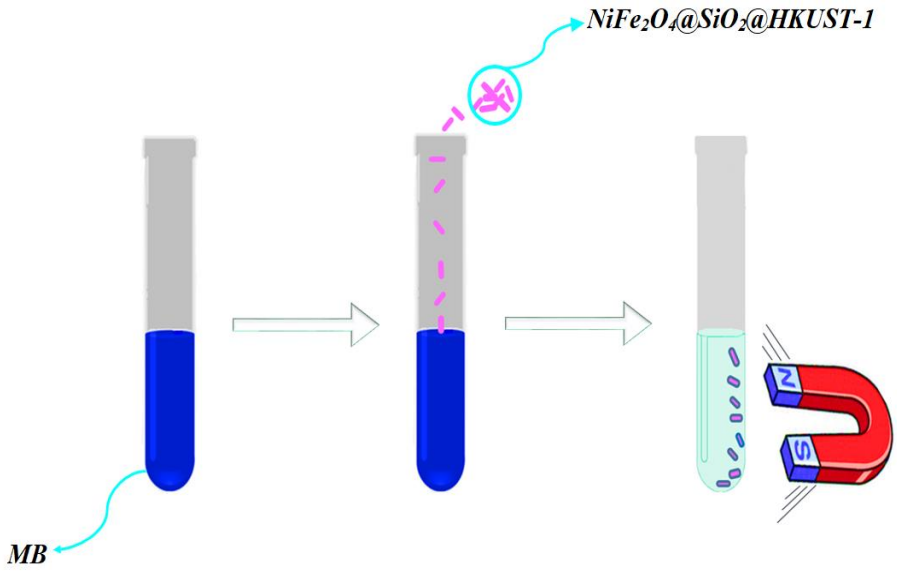

Fig. 12. Schematic of decolorization of methylene blue by magnetic metal-organic framework nanocomposites synthesized

at 10 ppm concentration is the highest amount such that after 60 minutes about 95% of dye was removed. However, for methylene blue dye solution with concentration (30 and 50 ppm), the removal efficiency reached (62.4% and 59.03%). This indicates that the removal efficiency decreased with increasing concentration of methylene blue dye solution. The reason for this decline is that as the concentration of the dye solution rises, the dye molecules in the solution increase, and given the constant concentration of the nanocomposite metal-organic framework synthesized in these solutions, the active sites and specific surface area of the nanocomposites are completely saturated and filled. As a result, the lower the concentration of the dye solution, the less the dye molecule in the solution. Consequently, the pore volumes and surface areas will be filled in a longer time and their removal efficiency will be higher.

pH Effect of dye solution on dye removal

To remove methylene blue pollutants from the dyeing effluent, methylene blue aqueous solution (10 ppm) was first prepared. Then, 100 ml of it was taken as a sample and its pH was measured using transcellular paper. And then, using dilute acid chloride (HCl) to acidify the pH and by using (KOH) to alkalinify the pH of the solutions. They were then examined to obtain the optimum pH. After reaching the desired pH, 1 ml of oxygenated water was added and finally 0.1 gr of nanocomposite metal-organic framework ($NiFe_2O_4$@SiO_2@HKUST-1) of 30 wt.% as adsorbent was added. It was subjected to ultrasonication for better mixing. Every 10 minutes a sample was taken and centrifuged, then, using a spectrophotometer, the wavelength was measured and the removal efficiency was calculated.

The results indicate that the dye removal on the metal organic framework would be different at different pHs. This difference is due to the charge of dye ions and the degradation properties by changing the pH of the solution. Following the decrease of pH (from alkaline to acidic), methylene blue dye removal increased because at acidic pH the concentration of H^+ and in the alkaline pH the concentration of OH increased in the solution and rising the concentration of these ions enhances or diminishes the removal efficiency of the dye. The results demonstrate that the acidic pH increased the efficiency of methylene blue dye removal due to the increased concentration of H^+ and the presence of hydrogen peroxide (H_2O_2) in the solution. In the alkaline pH range, the Fe (III) in the environment precipitates ($Fe(OH)_3$) and decomposes H_2O_2 into water and oxygen. In addition, the formation of iron (II) complexes at higher pH reduces its concentration in the environment; in contrast, the re-production of Fe (II) is prevented by the reaction of (Fe^{3+}) and (H_2O_2) at more acidic pHs; therefore, the acidic pH is considered as the optimum pH [64-69].

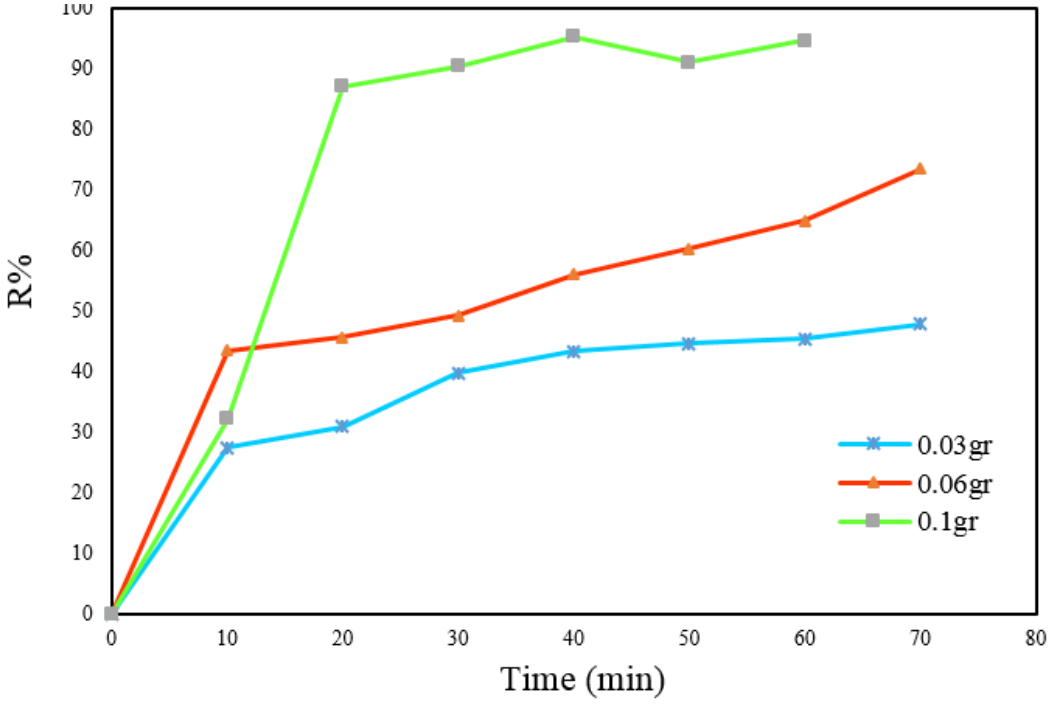

Fig. 13. Diagram of the effect of different concentrations nano composite on methylene blue degradation.

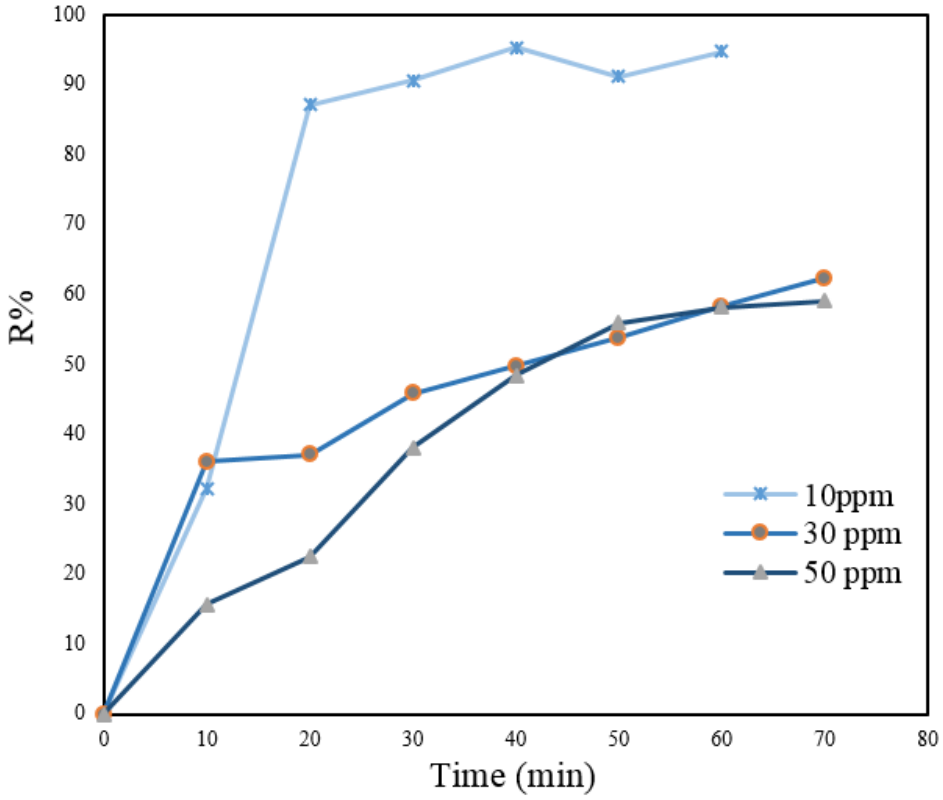

Fig. 14. Effect of dissolved concentration on degradation of methylene blue dyetion.

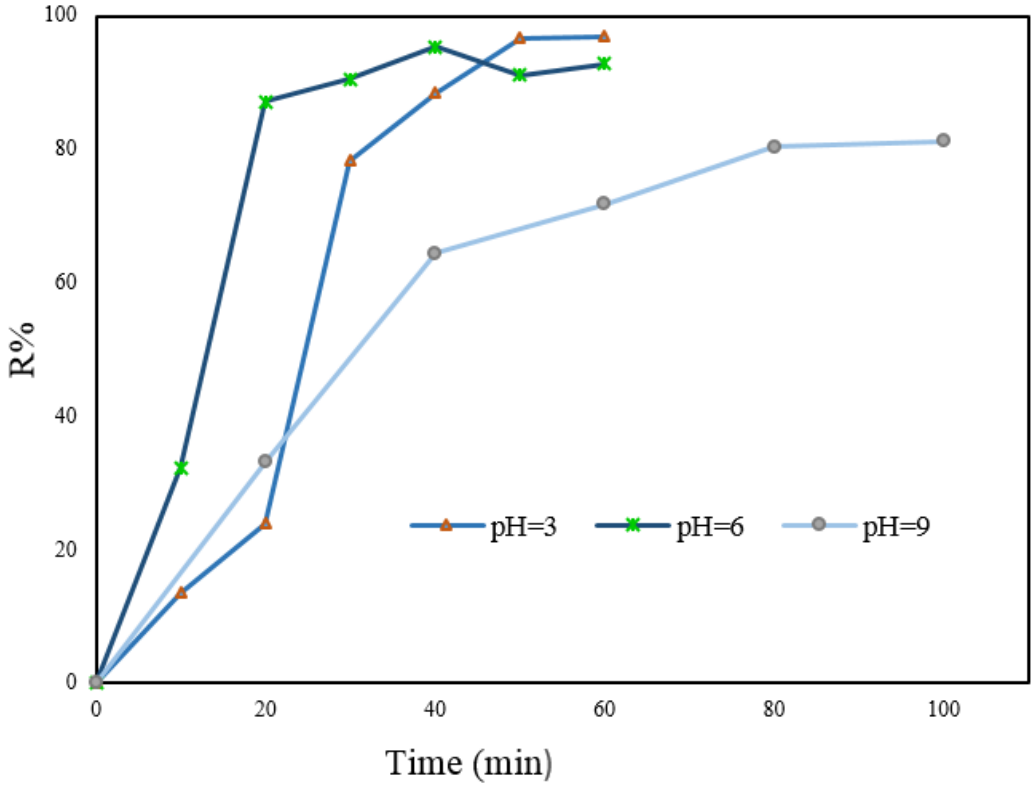

Fig. 15. Graph showing the effect of pH on the removal of methylene blue dye

Effect of ($NiFe_2O_4$)@SiO_2@ HKUST-1 amount

To remove methylene blue dye as an environmental contaminant from dyeing wastewater, methylene blue aqueous solution (10 mg/L) was first prepared, then 100 ml of it was taken as a sample and 0.1 gr of ($NiFe_2O_4$)@SiO_2@ HKUST-1 by 30, and 50 wt.% was added to the colored solution. In addition, 1 ml of oxygenated water (H_2O_2) was added and subjected to ultrasonication for complete mixing. Then every 10 minutes the sample was taken and centrifuged, and finally, using a spectrophotometer, their wavelengths were obtained. By using the resulting wavelengths, the values of the removal of any of the metal organic frameworks can be calculated over time.

As can be seen in Fig. (16), the synthesized 30% $NiFe_2O_4$@SiO_2)@HKUST-1 nanocomposite had the highest removal in a shorter time than the metal-organic framework nanocomposite of 50 wt.%. As a result, within 60 minutes approximately 98% of dye removal was observed. For this reason, the magnetic metal-organic framework nanocomposite 30% $NiFe_2O_4$@SiO_2@HKUST-1 was used in different conditions.

Kinetic studies

To study the removal behavior of dye, degradation mechanism, and rate of its removal, first- and second-rate kinetic equation and intramolecular infiltration were used to analyze the obtained data. Initially, different kinds of magnetic metal-organic framework nanocomposites synthesized with different weight percentages at different concentrations were examined. Then, the magnetic metal-organic framework with higher removal efficiency was investigated.

Kinetics of methylene blue dye degradation by magnetic metal-organic framework nanocomposites synthesized by weight percentages (30 and 50%) was investigated and calculated; furthermore, the methylene blue adsorption kinetics was studied at different concentrations of the solution (Fig. 17). Initially, the methylene blue degradation kinetics of metal-organic framework nanocomposites was calculated using pseudo-first-order kinetic by applying the following formula:

$$Ln\ (q_e - q_t) = Ln\ q_e - K_1 t$$

Where qe is the equilibrium adsorption ($mg.g^{-1}$) and qt is adsorption at different times

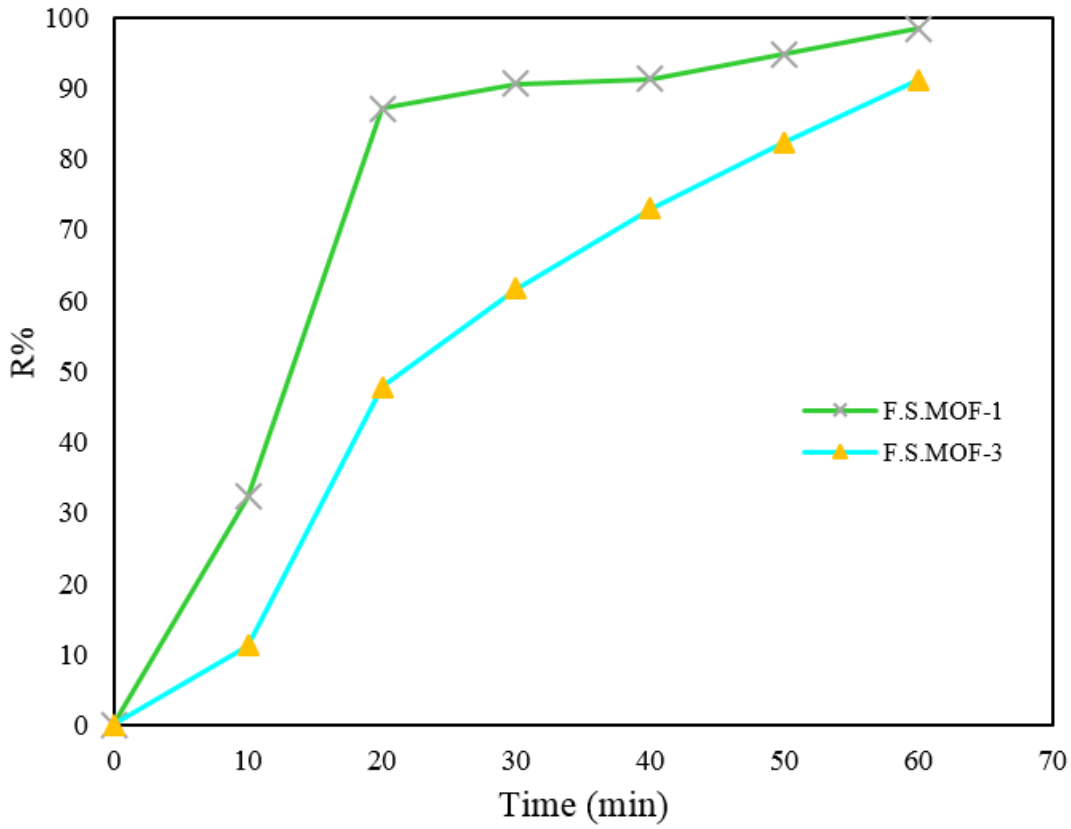

Fig. 16. Diagram of methylene blue dye removal using nanocomposites with different percentages of nickel ferrite in a silica substrate

($mg.g^{-1}$); k1 is the constant rate of absorption (min^{-1}) and t represents time. In the second step, the adsorption kinetics was calculated using the pseudo-second-order equation by the following equation:

$t/q = 1/K_2 q_{e\ 2} + t/q_e$

Where, like the above equation, K_2 is the rate of absorption constant (min^{-1}). The intramolecular diffusion kinetic method was employed to study the third kinetics, which can also be used to investigate the kinetics and compare the amount of dye penetrating into the nanocomposite molecules. The following equation was used for the intramolecular diffusion method:

$q_e = K_p t^{1/2} + I$

Where KP is the rate of diffusion within the molecule. Finally, by comparing these three kinetic models, it can be estimated which kinetic nickel-ferrous magnetic metal-organic nanocomposites in the silica substrate follow and its absorption rate can be calculated [64-70].

The pseudo-second-order kinetic model fits better than the other two models for synthesized metalorganic framework nanocomposites because, as calculated from the above equation, the coefficient of determination R^2 for the pseudo-second-order model is calculated and all coefficients are very close to one. Whereas the two pseudo-first-order models and the intramolecular diffusion are more distant than the second-order ones. Therefore, it can be concluded that the methylene blue dye kinetic using a variety of synthesized nanocomposites follows the pseudo-second-order kinetic. On the other hand, the amount of $(qe)_{cel}$ obtained from the above equations in the pseudo-second-order kinetic model is much closer to the empirical value of $(qe)_{ex}$. Table 6 presents the values of the coefficient of determination R^2 as well as the rate of degradation and the amount of degradation for each of the three kinetic models given. Table 7 shows the data obtained from the calculation of different kinetic models for different types of synthesized nanocomposites.

Among the synthesized nanocomposites,

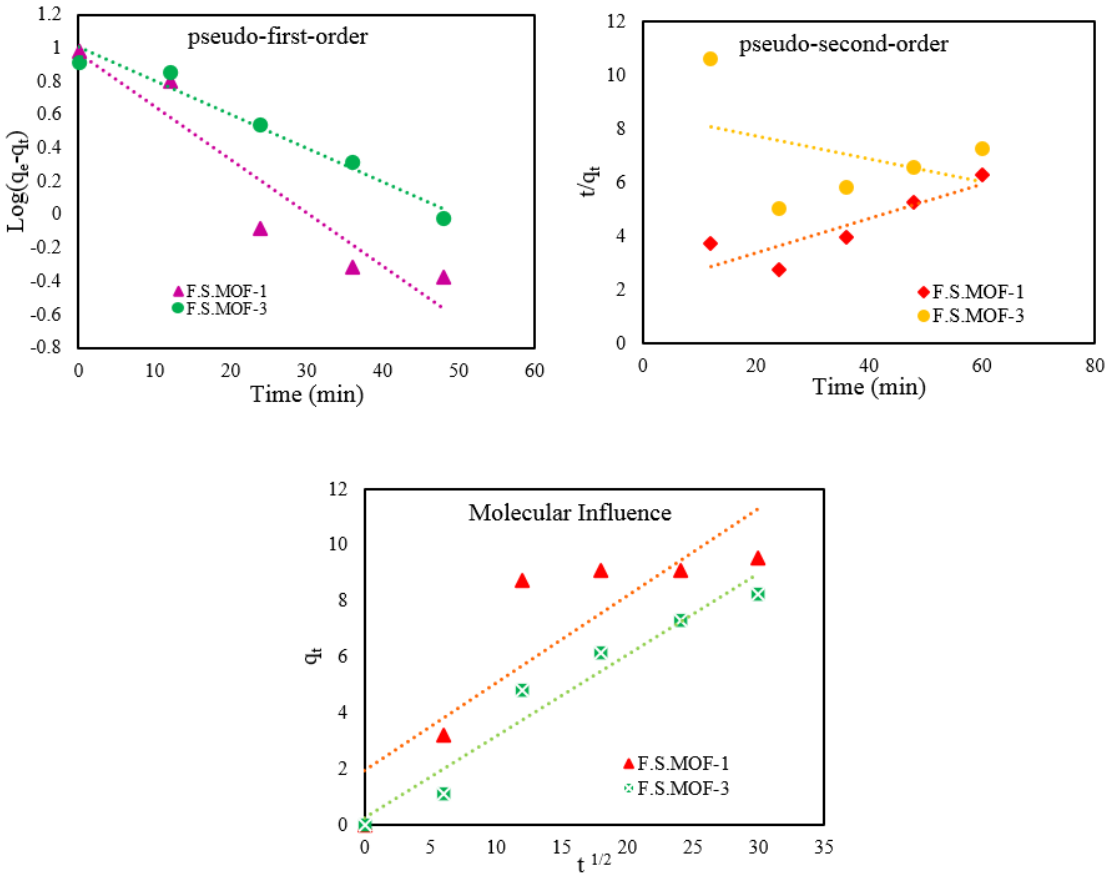

Fig. 17. Examination of different kinetic types for methylene blue degradation with different nanocomposites a) The pseudo-first-order kinetics b) pseudo-second-order kinetic c) kinetic of intramolecular penetration

the metal-organic nanocomposite ($NiFe_2O_4$@ SiO_2@ HKUST-1) with 30 wt.% showed better color removal. Consequently, the kinetics for this nanocomposite metal-organic framework was calculated at different concentrations of a solution. All the above models were studied to find the kinetics of these nanocomposites (Fig 18).

The pseudo-second-order kinetic model fits better than the other two models for the metal-organic $NiFe_2O_4$@SiO_2@HKUST-1 nanocomposite synthesized at x = 30 wt.%. Because, as calculated from the above equation for the determinant coefficient R^2 of the pseudo-second-order model, all the coefficients are very close to one. On the other hand, the value of R^2 for the other two models, pseudo-first-order and intramolecular infiltration, are more distant from 1. Therefore, it can be concluded that the methylene blue dye adsorption kinetic using the desired nanocomposites at different concentrations of the methylene blue dye solution follows pseudo-second-order kinetics [64-72]. However, the amount of (q_e)cal absorption obtained from the above equations in the kinetic pseudo-second-order absorption model is much closer to the empirical value of (q_e) exp. In Table 6, the values of the determination coefficient ($0R^2$), as well as the rate of absorption and the amount of adsorption for all three kinetic models considered, are calculated and presented in different concentrations of methylene blue dye.

Mechanism of removal of methylene blue

Methylene blue is a thiazine dye, which is a basic cationic dye in aqueous solutions. It tends to bind to the nanocomposite due to the negatively charged nature of the surface of nanocomposite. The adsorption of MB on $NiFe_2O_4$@SiO_2@ HKUST-1 adsorbent shows a good fit to the pseudo-second-order kinetics model, and intra particle diffusion is not the only speed-controlled

Table 6. Values of coefficient of determination R^2 and rate of degradation and the amount of degradation for each of the three kinetic models given

		Sample	
Model	Parameter	F.S.MOF-1	F-S-MOF-3
Pseudo-First-Order	$(q)_{ex}$	9.2363	10.085
	$(q)_{cel}$	9.534	8.24
	R^2	0.889	0.964
Pseudo-Second -Order	$(q)_{ex}$	9.2363	10.085
	$(q)_{cel}$	15.649	23.364
	R^2	0.764	0.141
Molecular Influence	K_p	0.3127	0.291
	I	1.9169	0.291
	R^2	0.7668	0.948

Table 7. Data obtained from calculation of different kinetic methylene blue models using F.S.MOF-1

		Sample		
Model	Parameter	F-S-MOF-1		
	Concentration (mg/L)	10	30	50
Pseudo-First-Order	$(q)_{ex}$	8.699	20.6347	43.351
	$(q)_{cel}$	9.478	17.475	30.081
	R^2	0.925	0.847	0.913
Pseudo-Second-Order	$(q)_{ex}$	8.699	20.6347	43.351
	$(q)_{cel}$	7.854	18.859	30.051
	R^2	0.903	0.983	0.900
Molecular Influence	K_p	0.873	1.481	4.061
	I	2.924	5.53	
	R^2	0.525	0.962	0.927

step. The Langmuir isotherm is more suitable for describing the adsorption behavior of MB and the results suggest that the adsorption is a spontaneous process. The removal mechanism of methylene blue dye from aqueous solution using a metal-organic framework nanocomposite containing magnetic nanoparticles after adsorption onto the nanocomposite surface and in the presence of hydrogen peroxide as a strong oxidant, is due to the presence of iron (II) and hydrogen peroxide in the radical hydroxide medium. The hydroxide radical rapidly and selectively attacks the organic structure of the dye and converts the organic compound into water, carbon dioxide, and inorganic ions. During this reaction, ferrous (II) ions are converted to ferric (III) and oxide ions. These results are in good agreement with previous reports [73].

$$H_2O_2 + Fe^{2+} \longrightarrow Fe^{3+} + OH^{\bullet} + OH^-$$

$$Fe^{3+} + H_2O_2 \longrightarrow Fe^{2+} + OOH^{\bullet} + H^+$$

$$MB\,H + OH^{\bullet} \longrightarrow MB^{\bullet} + H_2O$$

$$MB^{\bullet} + Fe^{3+} \longrightarrow MB^+ + Fe^{2+}$$

$$MB^+ + OH^- \longrightarrow MBOH$$

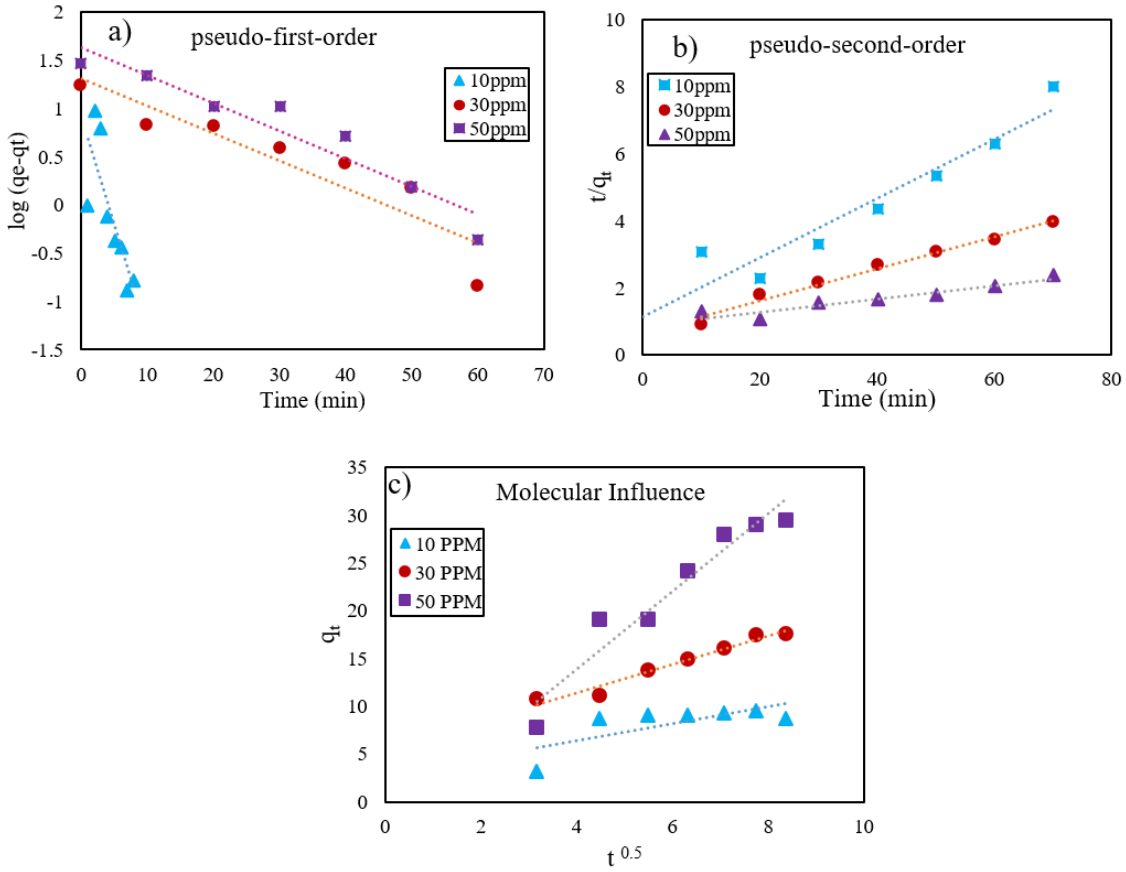

Fig. 18. kinetic study methylene blue using a metal-organic nanocomposite framework F.S.MOF-1 a) Kinetica of pseudo-first-order at different concentrations b) pseudo-second-order kinetic c) the intramolecular permeation kinetic.

CONCLUSION

In this study, $NiFe_2O_4$@SiO_2@HKUST-1 adsorbent was prepared by an in-situ self-assembly method, which is one of the green synthesis methods. In addition, $NiFe_2O_4$@SiO_2@HKUST-1 magnetic microspheres were characterized. The application of $NiFe_2O_4$@SiO_2@HKUST-1 in methylene blue pollutant adsorption and influence of time and pH factors were investigated. As a result, at more acidic pHs, the lower the concentration of the dye solution, the less the dye molecules in the solution. As a result, the pore volumes and surface areas will be filled in a longer time and their removal efficiency will be higher. As an optimum condition, within 60 minutes approximately 98% of dye removal was observed. For this reason, the magnetic metal-organic framework nanocomposite 30% $NiFe_2O_4$@SiO_2@HKUST-1 was employed as an optimum percentage which means that the adsorption process was mostly multilayered on heterogeneous surfaces of the metal-organic framework nanocomposites.

ACKNOWLEDGMENT

Authors acknowledge the Institute for Color Science and Technology for their support to carry out this study.

CONFLICT OF INTEREST

The authors declare no conflict of interest.

REFERENCES

1. Davari M, Bayat Kazazi S, Akbarzadeh Pivehzhani O. Nanomaterials: implications on agroecosystem. Nanotechnology: Springer; 2017. p. 59-71.
2. Akbarzadeh O, Mohd Zabidi NA, Abdullah B, Subbarao D. Synthesis and Characterization of Co/CNTs Catalysts Prepared by Strong Electrostatic Adsorption (SEA) Method. Applied Mechanics and Materials. 2014;625:328-32. 10.4028/www.scientific.net/AMM.625.328
3. Zhang W, Cue BW. Green techniques for organic synthesis

and medicinal chemistry: John Wiley & Sons; 2018.
4. Duan H, Wang D, Li Y. Green chemistry for nanoparticle synthesis. Chemical Society Reviews. 2015;44(16):5778-92. 10.1039/C4CS00363B
5. Julien PA, Mottillo C, Friščić T. Metal–organic frameworks meet scalable and sustainable synthesis. Green Chemistry. 2017;19(12):2729-47. 10.1039/C7GC01078H
6. Dreischarf AC, Lammert M, Stock N, Reinsch H. Green Synthesis of Zr-CAU-28: Structure and Properties of the First Zr-MOF Based on 2,5-Furandicarboxylic Acid. Inorganic Chemistry. 2017;56(4):2270-7. 10.1021/acs.inorgchem.6b02969
7. Lajevardi A, Tavakkoli Yaraki M, Masjedi A, Nouri A, Hossaini Sadr M. Green synthesis of MOF@Ag nanocomposites for catalytic reduction of methylene blue. Journal of Molecular Liquids. 2019;276:371-8. https://doi.org/10.1016/j.molliq.2018.12.002
8. Hunger K. Industrial dyes: chemistry, properties, applications: John Wiley & Sons; 2007.
9. Hassaan MA, El Nemr A, Hassaan A. Health and environmental impacts of dyes: mini review. American Journal of Environmental Science and Engineering. 2017;1(3):64-7.
10. Ismail M, Akhtar K, Khan MI, Kamal T, Khan MA, M. Asiri A, et al. Pollution, Toxicity and Carcinogenicity of Organic Dyes and their Catalytic Bio-Remediation. Current Pharmaceutical Design. 2019;25(34):3645-63. 10.2174/1381612825666191021142026
11. Katheresan V, Kansedo J, Lau SY. Efficiency of various recent wastewater dye removal methods: A review. Journal of Environmental Chemical Engineering. 2018;6(4):4676-97. https://doi.org/10.1016/j.jece.2018.06.060
12. Bhatia D, Sharma NR, Singh J, Kanwar RS. Biological methods for textile dye removal from wastewater: A review. Critical Reviews in Environmental Science and Technology. 2017;47(19):1836-76. 10.1080/10643389.2017.1393263
13. Austen V, Suyitno C, Gah TYPR, Sugiarta P, Santoso SP, Soetaredjo FE, et al. Fenton reagent for organic compound removal in wastewater. Fenton Reagent for Organic Compound Removal in Wastewater. 2020;3(1):1-16.
14. Singh S, Ransingh A. Coagulation and Electrocoagulation Process for Dye Removal from Textile Wastewater: A Review. CSVTU Research Journal on Engineering and Technology. 2020;9(01):29-41.
15. Wei F, Ren Q, Yang L, Wu L, Jian Q, Liang Z, et al. Adsorptive and Photocatalytic Dye Removal from Wastewater Using Metal-Organic Frameworks. IOP Conference Series: Materials Science and Engineering. 2020;782(5):052002. 10.1088/1757-899X/782/5/052002
16. Wang D, Jana D, Zhao Y. Metal–Organic Framework Derived Nanozymes in Biomedicine. Accounts of Chemical Research. 2020;53(7):1389-400. 10.1021/acs.accounts.0c00268
17. Cheng F, Marshall ES, Young AJ, Robinson PJ, Bouillard J-SG, Adawi AM, et al. Magnetic Control of MOF Crystal Orientation and Alignment. Chemistry – A European Journal. 2017;23(62):15578-82. https://doi.org/10.1002/chem.201703812
18. Wang L, Zeng T, Liao G, Cheng Q, Pan Z. Syntheses, structures and catalytic mechanisms of three new MOFs for aqueous Cr(VI) reduction and dye degradation under UV light. Polyhedron. 2019;157:152-62. https://doi.org/10.1016/j.poly.2018.09.064
19. Ishii T. Regulation of Genome Editing in Plant Biotechnology: Japan. In: Dederer H-G, Hamburger D, editors. Regulation of Genome Editing in Plant Biotechnology: A Comparative Analysis of Regulatory Frameworks of Selected Countries and the EU. Cham: Springer International Publishing; 2019. p. 239-62. 10.1007/978-3-030-17119-3_6
20. Sujing W, Serre C, Guillou N, Steunou N. Crystalline high degree of condensation titanium-based inorganic-organic hybrid solid MOF material, method for preparing same and uses thereof. Google Patents; 2021.
21. Kukulka W, Cendrowski K, Michalkiewicz B, Mijowska E. Correction: MOF-5 derived carbon as material for CO 2 adsorption. RSC advances. 2019;9(59):34349-.
22. Lee Y-R, Kim J, Ahn W-S. Synthesis of metal-organic frameworks: A mini review. Korean Journal of Chemical Engineering. 2013;30(9):1667-80. 10.1007/s11814-013-0140-6
23. Reinsch H. "Green" Synthesis of Metal-Organic Frameworks. European Journal of Inorganic Chemistry. 2016;2016(27):4290-9. https://doi.org/10.1002/ejic.201600286
24. Bon V, Senkovska I, Kaskel S. Metal-organic frameworks. Nanoporous Materials for Gas Storage: Springer; 2019. p. 137-72. 10.1007/978-981-13-3504-4_6
25. Jiao L, Seow JYR, Skinner WS, Wang ZU, Jiang H-L. Metal–organic frameworks: Structures and functional applications. Materials Today. 2019;27:43-68. https://doi.org/10.1016/j.mattod.2018.10.038
26. Kefeni KK, Msagati TAM, Mamba BB. Ferrite nanoparticles: Synthesis, characterisation and applications in electronic device. Materials Science and Engineering: B. 2017;215:37-55. https://doi.org/10.1016/j.mseb.2016.11.002
27. Kefeni KK, Mamba BB, Msagati TAM. Application of spinel ferrite nanoparticles in water and wastewater treatment: A review. Separation and Purification Technology. 2017;188:399-422. https://doi.org/10.1016/j.seppur.2017.07.015
28. Maksoud MIAA, El-Sayyad GS, Ashour AH, El-Batal AI, Elsayed MA, Gobara M, et al. Antibacterial, antibiofilm, and photocatalytic activities of metals-substituted spinel cobalt ferrite nanoparticles. Microbial Pathogenesis. 2019;127:144-58. https://doi.org/10.1016/j.micpath.2018.11.045
29. Liu F, Zhou K, Chen Q, Wang A, Chen W. Application of magnetic ferrite nanoparticles for removal of Cu(II) from copper-ammonia wastewater. Journal of Alloys and Compounds. 2019;773:140-9. https://doi.org/10.1016/j.jallcom.2018.09.240
30. Kefeni KK, Mamba BB. Photocatalytic application of spinel ferrite nanoparticles and nanocomposites in wastewater treatment: Review. Sustainable Materials and Technologies. 2020;23:e00140. https://doi.org/10.1016/j.susmat.2019.e00140
31. Nikolić VN, Tadić M, Panjan M, Kopanja L, Cvjetićanin N, Spasojević V. Influence of annealing treatment on magnetic properties of Fe2O3/SiO2 and formation of ε-Fe2O3 phase. Ceramics International. 2017;43(3):3147-55. https://doi.org/10.1016/j.ceramint.2016.11.132
32. Zheng J, Liu ZQ, Zhao XS, Liu M, Liu X, Chu W. One-step solvothermal synthesis of Fe3O4@C core–shell nanoparticles with tunable sizes. Nanotechnology. 2012;23(16):165601. 10.1088/0957-4484/23/16/165601
33. Surowiec Z, Budzyński M, Durak K, Czernel G. Synthesis and characterization of iron oxide magnetic nanoparticles. Nukleonika. 2017;62. 10.1515/nuka-2017-0009
34. Huang L, Cai J, He M, Chen B, Hu B. Room-Temperature

Synthesis of Magnetic Metal–Organic Frameworks Composites in Water for Efficient Removal of Methylene Blue and As(V). Industrial & Engineering Chemistry Research. 2018;57(18):6201-9. 10.1021/acs.iecr.7b05294
35. Bellusci M, Guglielmi P, Masi A, Padella F, Singh G, Yaacoub N, et al. Magnetic Metal–Organic Framework Composite by Fast and Facile Mechanochemical Process. Inorganic Chemistry. 2018;57(4):1806-14. 10.1021/acs.inorgchem.7b02697
36. Shi Z, Xu C, Guan H, Li L, Fan L, Wang Y, et al. Magnetic metal organic frameworks (MOFs) composite for removal of lead and malachite green in wastewater. Colloids and Surfaces A: Physicochemical and Engineering Aspects. 2018;539:382-90. https://doi.org/10.1016/j.colsurfa.2017.12.043
37. Ding T, Zhang S, Zhang W, Zhang G, Gao Z-W. Highly selective C2H2 and CO2 capture and magnetic properties of a robust Co-chain based metal–organic framework. Dalton Transactions. 2019;48(22):7938-45. 10.1039/C9DT00510B
38. Abdi J, Mahmoodi NM, Vossoughi M, Alemzadeh I. Synthesis of magnetic metal-organic framework nanocomposite (ZIF-8@SiO2@MnFe2O4) as a novel adsorbent for selective dye removal from multicomponent systems. Microporous and Mesoporous Materials. 2019;273:177-88. https://doi.org/10.1016/j.micromeso.2018.06.040
39. Thanh HTM, Tu NTT, Hung NP, Tuyen TN, Mau TX, Khieu DQ. Magnetic iron oxide modified MIL-101 composite as an efficient visible-light-driven photocatalyst for methylene blue degradation. Journal of Porous Materials. 2019;26(6):1699-712. 10.1007/s10934-019-00767-1
40. Saemian T, Gharagozlou M, Hossaini Sadr M, Naghibi S. Synthesis of CoFe2O4@Cu3(BTC)2 nanocomposite as a magnetic metal–organic framework. Polyhedron. 2019;174:114163. https://doi.org/10.1016/j.poly.2019.114163
41. Xu T, Hou X, Liu S, Liu B. One-step synthesis of magnetic and porous Ni@MOF-74(Ni) composite. Microporous and Mesoporous Materials. 2018;259:178-83. https://doi.org/10.1016/j.micromeso.2017.10.014
42. Hossein Zadeh M, Keramati N, Mehdipour Ghazi M. The effect of solvents on photocatalytic activity of Fe-BTC metal organic framework obtained via sonochemical method. Inorganic and Nano-Metal Chemistry. 2019;49(12):448-54. 10.1080/24701556.2019.1661455
43. Szalad H, Candu N, Cojocaru B, Păsătoiu TD, Andruh M, Pârvulescu VI. ∞3[Cu2(mand)2(hmt)]–MOF: A Synergetic Effect between Cu(II) and Hexamethylenetetramine in the Henry Reaction. Chemistry [Internet]. 2020; 2(1):[50-62 pp.]. 10.3390/chemistry2010006
44. Bhardwaj SK, Bhardwaj N, Mohanta GC, Kumar P, Sharma AL, Kim K-H, et al. Immunosensing of Atrazine with Antibody-Functionalized Cu-MOF Conducting Thin Films. ACS Applied Materials & Interfaces. 2015;7(47):26124-30. 10.1021/acsami.5b07692
45. Zhang L, Sun J, Zhou Y, Zhong Y, Ying Y, Li Y, et al. Layer-by-layer assembly of Cu3(BTC)2 on chitosan non-woven fabrics: a promising haemostatic decontaminant composite material against sulfur mustard. Journal of Materials Chemistry B. 2017;5(30):6138-46. 10.1039/C7TB01489A
46. Musić S, Filipović-Vinceković N, Sekovanić L. Precipitation of amorphous SiO2 particles and their properties. Brazilian journal of chemical engineering. 2011;28:89-94. .org/10.1590/S0104-66322011000100011
47. Naidu TM, Narayana PL. Synthesis and Characterization of Fe-TiO 2 and NiFe 2 O 4 Nanoparticles and Its Thermal Properties. Journal of Nanoscience and Technology. 2019:769-72. 10.30799/jnst.247.19050407
48. Patel S, Saleem M, Varshney D, editors. Structural and optical properties of NiFe2O4 synthesized via green technology. AIP Conference Proceedings; 2018: AIP Publishing LLC. 10.1063/1.5032429
49. Perez E, Gomez-Polo C, Larumbe S, Perez-Landazabal J, Sagredo V. Structural and magnetic properties of NiFe2 O4 and NiFe2 O4/SiO2 nanoparticles prepared by Sol-Gel combustion. Revista Mexicana de Física. 2012;58(2):104-7.
50. Fu H, Ding X, Ren C, Li W, Wu H, Yang H. Preparation of magnetic porous NiFe 2 O 4/SiO 2 composite xerogels for potential application in adsorption of Ce (iv) ions from aqueous solution. RSC Advances. 2017;7(27):16513-23. 10.1039/C6RA27219C
51. Xu X. Controllable synthesis of ultra-small metal–organic framework nanocrystals composed of copper(ii) carboxylates. Nanoscale. 2016;8(37):16725-32. 10.1039/C6NR05639C
52. Todaro M AA, Sciortino L, Agnello S, Cannas M, Mario Gelardi F, Buscarino G. Investigation by Raman Spectroscopy of the Decomposition Process of HKUST-1 upon Exposure to Air. Journal of Spectroscopy. 2016;2016:8074297 10.1155/2016/8074297
53. Gharagozlou M. New Synthesis and Magnetic Properties of NiFe2O4/SiO2 and Co0.5Zn0.5Fe2O4/SiO2 Nanocomposites Using Tetraglycolatosilane as Precursor. Journal of the Chinese Chemical Society. 2012;59(7):884-90. https://doi.org/10.1002/jccs.201100606
54. Cao J, Su Y, Liu Y, Guan J, He M, Zhang R, et al. Self-assembled MOF membranes with underwater superoleophobicity for oil/water separation. Journal of Membrane Science. 2018;566:268-77. https://doi.org/10.1016/j.memsci.2018.08.068
55. Bedia J, Muelas-Ramos V, Peñas-Garzón M, Gómez-Avilés A, Rodríguez JJ, Belver C. A Review on the Synthesis and Characterization of Metal Organic Frameworks for Photocatalytic Water Purification. Catalysts [Internet]. 2019; 9(1). 10.3390/catal9010052
56. Xu Y, Jin J, Li X, Han Y, Meng H, Wang T, et al. Fabrication of hybrid magnetic HKUST-1 and its highly efficient adsorption performance for Congo red dye. RSC Advances. 2015;5(25):19199-202. 10.1039/C5RA00384A
57. Wang Y, Nie S, Liu Y, Yan W, Lin S, Cheng G, et al. Room-Temperature Fabrication of a Nickel-Functionalized Copper Metal–Organic Framework (Ni@Cu-MOF) as a New Pseudocapacitive Material for Asymmetric Supercapacitors. Polymers [Internet]. 2019; 11(5). 10.3390/polym11050821
58. Zhang R, Tao C-A, Chen R, Wu L, Zou X, Wang J. Ultrafast Synthesis of Ni-MOF in One Minute by Ball Milling. Nanomaterials [Internet]. 2018; 8(12). 10.3390/nano8121067
59. Pangestu T, Kurniawan Y, Soetaredjo FE, Santoso SP, Irawaty W, Yuliana M, et al. The synthesis of biodiesel using copper based metal-organic framework as a catalyst. Journal of Environmental Chemical Engineering. 2019;7(4):103277. https://doi.org/10.1016/j.jece.2019.103277
60. Han T, Li C, Guo X, Huang H, Liu D, Zhong C. In-situ synthesis of SiO2@MOF composites for high-efficiency removal of aniline from aqueous solution. Applied Surface Science. 2016;390:506-12. https://doi.org/10.1016/j.

apsusc.2016.08.111
61. Naghibi S, Madaah Hosseini HR, Faghihi Sani MA, Shokrgozar MA, Mehrjoo M. Mortality response of folate receptor-activated, PEG–functionalized TiO2 nanoparticles for doxorubicin loading with and without ultraviolet irradiation. Ceramics International. 2014;40(4):5481-8. https://doi.org/10.1016/j.ceramint.2013.10.136
62. Mitra S, Mandal K, Anil Kumar P. Temperature dependence of magnetic properties of NiFe2O4 nanoparticles embeded in SiO2 matrix. Journal of Magnetism and Magnetic Materials. 2006;306(2):254-9. https://doi.org/10.1016/j.jmmm.2006.03.024
63. Almessiere MA, Slimani Y, Güner S, Baykal A, Ercan I. Effect of dysprosium substitution on magnetic and structural properties of NiFe2O4 nanoparticles. Journal of Rare Earths. 2019;37(8):871-8. https://doi.org/10.1016/j.jre.2018.10.009
64. Zhao R, Wang Y, Li X, Sun B, Wang C. Synthesis of β-Cyclodextrin-Based Electrospun Nanofiber Membranes for Highly Efficient Adsorption and Separation of Methylene Blue. ACS Applied Materials & Interfaces. 2015;7(48):26649-57. 10.1021/acsami.5b08403
65. Aksu Z. Application of biosorption for the removal of organic pollutants: a review. Process Biochemistry. 2005;40(3):997-1026. https://doi.org/10.1016/j.procbio.2004.04.008
66. Li Q, Li Y, Ma X, Du Q, Sui K, Wang D, et al. Filtration and adsorption properties of porous calcium alginate membrane for methylene blue removal from water. Chemical Engineering Journal. 2017;316:623-30. https://doi.org/10.1016/j.cej.2017.01.098
67. Gong J-L, Wang B, Zeng G-M, Yang C-P, Niu C-G, Niu Q-Y, et al. Removal of cationic dyes from aqueous solution using magnetic multi-wall carbon nanotube nanocomposite as adsorbent. Journal of Hazardous Materials. 2009;164(2):1517-22. https://doi.org/10.1016/j.jhazmat.2008.09.072
68. Liu S, Ding Y, Li P, Diao K, Tan X, Lei F, et al. Adsorption of the anionic dye Congo red from aqueous solution onto natural zeolites modified with N,N-dimethyl dehydroabietylamine oxide. Chemical Engineering Journal. 2014;248:135-44. https://doi.org/10.1016/j.cej.2014.03.026
69. Tara N, Siddiqui SI, Rathi G, Chaudhry SA, Inamuddin, Asiri AM. Nano-engineered Adsorbent for the Removal of Dyes from Water: A Review. Current Analytical Chemistry. 2020;16(1):14-40. 10.2174/1573411015666190117124344
70. Shao Y, Zhou L, Bao C, Ma J, Liu M, Wang F. Magnetic responsive metal–organic frameworks nanosphere with core–shell structure for highly efficient removal of methylene blue. Chemical Engineering Journal. 2016;283:1127-36. https://doi.org/10.1016/j.cej.2015.08.051
71. Deng H, Grunder S, Cordova KE, Valente C, Furukawa H, Hmadeh M, et al. Large-Pore Apertures in a Series of Metal-Organic Frameworks. Science. 2012;336(6084):1018-23. 10.1126/science.1220131
72. Zheng S, Li X, Yan B, Hu Q, Xu Y, Xiao X, et al. Transition-Metal (Fe, Co, Ni) Based Metal-Organic Frameworks for Electrochemical Energy Storage. Advanced Energy Materials. 2017;7(18):1602733. https://doi.org/10.1002/aenm.201602733
73. Chen D, Zeng Z, Zeng Y, Zhang F, Wang M. Removal of methylene blue and mechanism on magnetic γ-Fe2O3/SiO2 nanocomposite from aqueous solution. Water Resources and Industry. 2016;15:1-13. https://doi.org/10.1016/j.wri.2016.05.003